OPEN ACCESS



Triples as Links between Binary Black Hole Mergers, Their Electromagnetic Counterparts, and Galactic Black Holes

Smadar Naoz 1,2 , Zoltán Haiman 3,4,5 , Eliot Quataert , and Liz Holzknecht 1,2 , and Liz Holzkn

Abstract

We propose a formation pathway linking black holes (BHs) observed in gravitational-wave (GW) mergers, wide BH-stellar systems uncovered by Gaia, and accreting low-mass X-ray binaries (LMXBs). In this scenario, a stellar-mass BH binary undergoes isolated binary evolution and merges while hosting a distant, dynamically unimportant tertiary stellar companion. The tertiary becomes relevant only after the merger, when the remnant BH receives a GW recoil kick. Depending on the kick velocity and system configuration, the outcome can be: (1) a bright electromagnetic (EM) counterpart to the GW merger; (2) an LMXB; (3) a wide BH-stellar companion system resembling the Gaia BH population; or (4) an unbound isolated BH. Modeling the three-body dynamics, we find that $\sim\!0.02\%$ of LIGO-Virgo-KAGRA (LVK) mergers may be followed by an EM counterpart within $\sim\!10\,\mathrm{days}$, produced by tidal disruption of the star by the BH. The flare is likely brightest in the optical-UV and lasts for days to weeks; in some cases, partial disruption causes recurring flares with a period of $\sim\!2$ months. We further estimate that this channel can produce $\sim\!1\%\!-\!10\%$ of Gaia BH systems in the Milky Way. This scenario provides the first physically motivated link between GW sources, Gaia BHs, and some X-ray binaries, and predicts a rare but robust pathway for EM counterparts to binary BH mergers, potentially detectable in LVK's O5 run.

Unified Astronomy Thesaurus concepts: Black holes (162); Gravitational wave sources (677); Gravitational waves (678); LIGO (920); Stellar mass black holes (1611); Low-mass x-ray binary stars (939); Gaia (2360)

1. Introduction

Stellar-mass black holes (BHs) can be detected through multiple observational methods, each of which potentially probes different evolutionary pathways. The oldest method relies on electromagnetic (EM) signatures, most notably X-ray emission from accretion disks in X-ray binaries (XRBs). These systems, discovered in the 1960s, provided the first indirect evidence for stellar-mass BHs (e.g., C. T. Bolton 1972; R. A. Remillard & J. E. McClintock 2006; M. MacLeod & J. Grindlay 2023). More recently, the detection of gravitational waves (GWs) from merging binary BHs by the LIGO-Virgo-KAGRA (LVK) Collaboration has revolutionized our understanding of the BH mass distribution (e.g., B. P. Abbott et al. 2016), revealing a population of heavy BHs (up to $\sim 100 \, M_{\odot}$) without any known EM activity. The third avenue of detection, based on astrometric measurements of orbital motion, has been enabled by Gaia, which has opened a new observational window onto detached BH binaries (K. El-Badry et al. 2023b). Stellar-mass BHs can also be detected by microlensing (e.g., E. Agol et al. 2002; J. R. Lu et al. 2016; C. Y. Lam et al. 2022; K. C. Sahu et al. 2022) or by combined

Original content from this work may be used under the terms of the Creative Commons Attribution 4.0 licence. Any further distribution of this work must maintain attribution to the author(s) and the title of the work, journal citation and DOI.

radial velocity and photometric observations of nonaccreting BHs in binaries (e.g., J. Liu et al. 2019b; T. A. Thompson et al. 2019; M. Clavel et al. 2021; C. Chawla et al. 2024), but our focus in this Letter is on the first three channels summarized above.

In addition to Gaia BH1 (K. El-Badry et al. 2023b), two additional candidates have been identified in Gaia DR3 astrometric solutions (Gaia Collaboration et al. 2021, 2023, 2024; K. El-Badry et al. 2023a), further demonstrating the potential of this technique to uncover detached BH binaries. However, the properties of Gaia BH1 in particular pose a significant evolutionary challenge: the orbital separation of the system lies in the range expected for the progenitor's red supergiant phase, where the envelope would have engulfed the companion and likely led to a common-envelope phase (K. El-Badry et al. 2023b).

While each of these populations provides complementary information, the connections between them remain poorly understood. Do the merging BH binaries observed by LVK originate from the same progenitors as the XRBs seen in the Galaxy? Are Gaia BHs an evolutionary link, or do they represent a distinct population? Reconciling the demographics and evolutionary pathways of these BH populations is a major open question, with implications for binary stellar evolution, supernova physics, and the formation of merging compact-object binaries.

Recent efforts have begun to explore this question using both population synthesis and targeted observations, but a coherent picture has yet to emerge (e.g., G. Wiktorowicz et al. 2019; M. Zevin et al. 2021; M. Fishbach & V. Kalogera 2022;

⁷ A handful of LVK BHs have been suggested to coincide with EM flares in AGNs (M. J. Graham et al. 2023; X. Huang et al. 2025), but their brightness is difficult to explain (H. Tagawa et al. 2024), and the significances of the spatial associations are controversial (N. Veronesi et al. 2025).

M. Fishbach et al. 2025). For example, M. Zevin et al. (2021) analyzed the second LIGO-Virgo catalog using population models for multiple BH binary formation pathways. They found that the diversity of the observed mergers is best explained by a mixture of channels rather than a single formation mechanism producing more than $\sim 70\%$ of the detected population; they also highlighted how assumptions about natal spins and common-envelope evolution strongly affect inferred branching fractions. Similarly, M. Fishbach & V. Kalogera (2022) compared the BHs in XRBs with those in GW-detected binary BHs. They showed that differences in masses between the BHs in GW events and XRBs can largely be explained by observational selection effects and binary mass correlations, with natal BH kicks possibly also playing a role (M. Fishbach et al. 2025). However, they also found a significant tension in the spin distributions, suggesting that while some binary BHs may have evolutionary histories similar to those of XRBs, others likely form through distinct channels.

In this Letter, we investigate whether the high prevalence of triples among massive stars (≥70%; M. Moe & R. Di Stefano 2017) can naturally connect the populations of BHs observed astrometrically, electromagnetically, and via GWs. In our scenario, when the inner BH binary in a hierarchical triple merges, the tertiary companion can remain bound, producing a wide BH binary detectable by Gaia or, in other cases, it can undergo mass transfer, leading to an XRB phase. In some cases, the tertiary companion is tidally disrupted, potentially producing luminous EM afterglows promptly following the merger. This triple-mediated evolutionary pathway therefore provides a unified framework that can produce Gaia BH systems, XRBs, and merging binary BHs, helping to explain the diversity and relative abundances of the observed BH populations. It also provides a robust, albeit rare, channel for producing EM counterparts to binary BH mergers. Figure 1 illustrates the different channels we consider and their connections.

We stress that while hierarchical triples have been proposed as a formation channel for merging binary BHs in the field, their overall contribution to the LVK-detected merger rate is typically estimated to be small and suppressed by a factor of \sim 5-30 relative to the estimated detected rate (e.g., F. Antonini et al. 2016, 2017; K. Silsbee & S. Tremaine 2017; B. Liu et al. 2019a; A. Dorozsmai et al. 2024; F. Kummer et al. 2025). Although it is important to note that each of these studies has surveyed a limited part of the parameter space, triple evolution may nonetheless naturally account for certain systems that are otherwise difficult to explain, such as BH mergers in the mass gap and other puzzles (e.g., W. Lu et al. 2021; A. Vigna-Gómez et al. 2021; M. A. S. Martinez et al. 2022; A. Dorozsmai et al. 2025). In this work, however, we focus on a complementary scenario: BH binaries that merge through isolated binary evolution, with a tertiary companion that does not play a significant dynamical role in driving the merger. In particular, the tertiary star's presence is relevant only after the inner binary merges, when the system receives a recoil kick. Our setup, therefore, explores the consequences of a passive tertiary in an otherwise binary-driven channel. We assume throughout this Letter that the distant tertiary companion remains bound during the formation of the two BHs in the inner binary, and we focus on the dynamics that follow when the inner BH binary merges. The validity of this assumption is sensitive, of course, to the

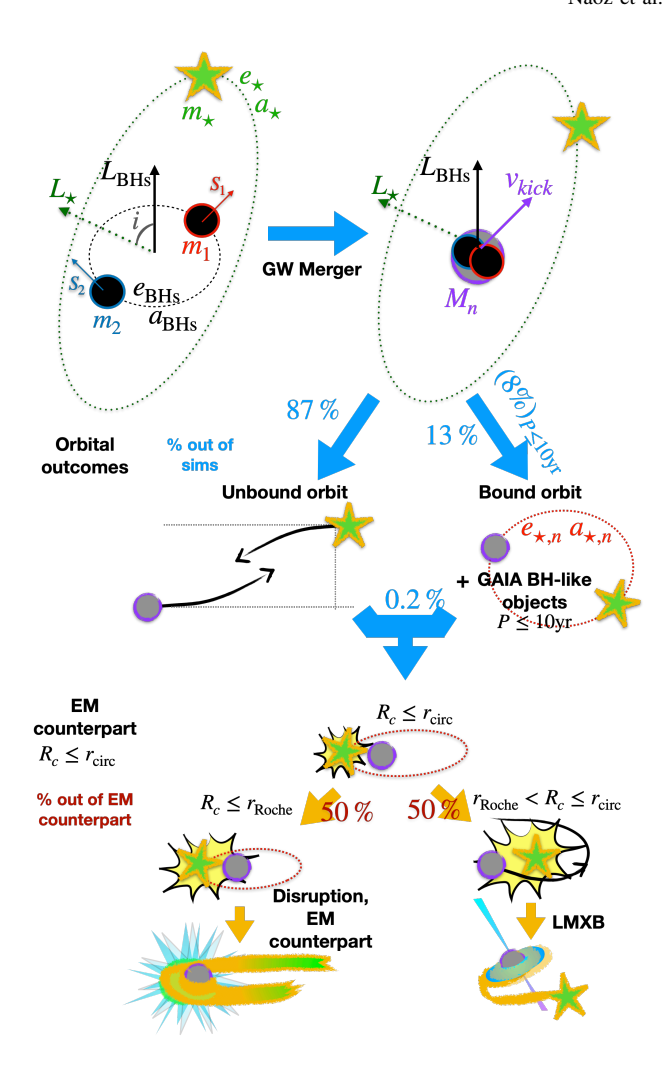


Figure 1. An illustration of the system. The three-body system is composed of two stellar-mass BHs and a distant main-sequence stellar tertiary. The angle between the first (second) BH's spin, S_1 (S_2) and the inner binary angular momentum $L_{\rm BHs}$ is i_{s1} (i_{s2}), and the angle in the plane of the orbit, measured from the semimajor axis, is φ_1 (φ_2). Finally, the angle between the inner binary angular momentum and the recoil kick vector is α . Post-recoil-kick, there are two possible outcomes: unbound orbits (87% of all systems) and bound orbits (13% of all systems). We highlight that 8% of all systems are bound with a period shorter than 10 yr, which are Gaia-BH-like systems. In 0.2% of all cases, either a bound or an unbound system results in an EM counterpart. These are designated by having the closest approach $R_c \leq r_{\rm circ}$, where 97.6% (2.4%) of all EM-bright sources are on a bound (unbound) orbit when they cross $r_{\rm circ}$. About 50% of these systems have a closest approach smaller than r_{Roche} , resulting in a prompt disruption event and yielding an EM counterpart to the GW emission with a time delay of about 10 days. Finally, 50% of the EM signatures have $r_{\text{Roche}} < R_c \leqslant r_{\text{circ}}$, which may result in an LMXB. Note that as stars evolve beyond the main sequence and become red giants, their radius expands, yielding a larger fraction of systems undergoing mass transfer events. We discuss these probabilities in detail in Section 4.2.

uncertain mass ejection and natal kick during BH formation. Recent detections of XRBs with distant companions imply that at least some distant companions remain bound during BH formation (e.g., K. B. Burdge et al. 2024; C. Shariat et al. 2025b).

This Letter is organized as follows. We begin by describing the system setup in Section 2. In Section 2.2, we provide a clear explanation of the effects of a kick on stellar orbits. To test the scenario, we conduct a proof-of-concept population study in Section 3. We use this population to estimate the rate

and detectability of EM signatures in Section 4.2 and Gaia BH detections in Section 4.3. Finally, we present our discussion and conclusions in Section 5.

2. System Setup and Equations

2.1. The Triple Configuration

Throughout this work, we consider a stellar-mass BH binary, m_1 and m_2 , where the mass ratio is $q \equiv m_1/m_2 \leqslant 1$, where "1" stands for the less massive component. The total mass of the binary is $M = m_1 + m_2$, with semimajor axis $a_{\rm BHs}$ and eccentricity $e_{\rm BH}$, associated with angular momentum $L_{\rm BHs}$. We define the spin-orbit angle of mass m_i as $i_{si} = \hat{h} \cdot \hat{S}_i$, where \hat{h} is the unit vector along the BH's orbital angular momentum, and $j \in \{1, 2\}$. The corresponding spherical coordinate angles are Ω_{si} for each mass. Further, this binary is orbited by a star with a mass $m_{\star} = 1 M_{\odot}$ and semimajor axis a_{\star} and eccentricity e_{\star} . We note that while triples are observed to have a twin excess (C. Shariat et al. 2025a), the long lifetime of $1 M_{\odot}$ benefits the calculation. In other words, the star is less likely to evolve before the BH binary merges. A full initial mass function (IMF) calculation for the tertiary mass is beyond the scope of this Letter. The frame of reference considered here is the inertial frame, for which the z-axis is parallel to the total angular momentum. After the BHs merge, they typically receive a recoil kick due to the anisotropic emission of GWs.

2.2. Impact on the Stellar Orbit

We adopt the C. O. Lousto et al. (2010, 2012) fitting formulae, which provide the recoil kick velocity. See the Appendix for the relevant set of equations. In this Letter, we focus on the merger channel driven by binary stellar evolution. This channel implies that the BH spins are aligned with its angular momentum. As a result, a well-known outcome emerges: the recoil kick is directed within the plane of the BH binary (e.g., C. O. Lousto et al. 2012). Note that since natal kicks may induce misalignment, the recoil kick may be tens of degrees off-axis. We discuss the effects of the spin alignment approximation in Section 4.3.

Assuming that the kick is instantaneous implies that the star and the new BH's separation does not change, i.e., $r = r_{\text{new}}$, and that they now have a velocity vector: $\mathbf{v}_{\text{new}} = \mathbf{v}_r - \mathbf{v}_{\text{kick}}$, where \mathbf{v}_r is the velocity vector of the outer binary just before the kick took place. The kick can either unbind the star–new BH system or alter its orbital configuration.

We can estimate the closest approach considering gravitational focusing:

$$b^{2} = R_{c}^{2} + R_{c} \frac{2G(m_{\star} + M_{\text{new}})}{v_{\text{new}}^{2}},$$
 (1)

where M_{new} is the post-merger BH mass computed from C. O. Lousto et al. (2010). This impact parameter is found using the post-kick velocity vector and separation:

$$b = r \sin \gamma$$
 where $\sin \gamma = \frac{|\nu_{\text{new}} \times r|}{|\nu_{\text{new}}||r|}$. (2)

Solving for R_c , we have:

$$R_c = \sqrt{b^2 + \frac{G^2(m_{\star} + M_{\text{new}})^2}{v_{\text{new}}^4} - \frac{G(m_{\star} + M_{\text{new}})}{v_{\text{new}}^2}}.$$
 (3)

Clearly, when $b \ll G(m_{\star} + M_{\rm new})/v_{\rm new}^2$, the resulting R_c will be small. This implies that for an arbitrary r, the post-kick binary velocity, $v_{\rm new}$, should be close to parallel to the star's separation vector. Generally, the parameter $\sin \gamma$ can be written as

$$\sin^2 \gamma = 1 - \frac{(\nu_{\text{new}} \cdot r)^2}{\nu_{\text{new}}^2 r^2},\tag{4}$$

where $v_{\text{new}} \cdot \mathbf{r} = (v_r - v_{\text{kick}}) \cdot \mathbf{r}$.

To gain insight for the expected result, consider a situation where the recoil kick takes place when the star is at its apocenter (or pericenter), thus $\mathbf{v}_r \cdot \mathbf{r} = 0$. Therefore, Equation (4) takes the following form:

$$\sin^2 \gamma = 1 - \frac{u_k^2 \cos^2 \alpha}{1 + u_k^2 - 2u_k \cos \theta} \quad \text{at apo/peri-center}, (5)$$

where we define the normalized velocity as $u_k \equiv v_{\rm kick}/v_r$, $v_r \cdot v_{\rm kick} = v_r v_{\rm kick} \cos \theta$, and $v_{\rm kick} \cdot r = r v_{\rm kick} \cos \alpha$. Note that based on the geometry of the system,

$$\eta - \theta \leqslant \alpha \leqslant \theta + \eta, \tag{6}$$

where $\cos \eta = \mathbf{v}_r \cdot \mathbf{r}/(\mathbf{v}_r r)$. At the apocenter/pericenter, $\eta = 90^\circ$. Thus, in the apocenter/pericenter case, $\sin \alpha = \cos \theta$. Achieving small R_c implies $\sin \gamma \to 0$; thus, we solve Equation (5)—in this case:

$$1 + u_k^2 \cos^2 \theta - 2u_k \cos \theta = 0$$
 at apocenter/pericenter. (7)

A straightforward solution occurs when $\theta=0^\circ$ and $u_k=1$. This means that the recoil velocity vector is directly parallel to the star's (pre-kick) velocity vector and has the same magnitude. In this scenario, we can expect $\sin\gamma\to 0$, which implies a small value for R_c . This situation also emphasizes the importance of the angle θ in determining the orbital configuration after the kick. This behavior is depicted in Figure 2, top panel, where for most values of q, we have $\theta\approx 0^\circ$. Considering two example systems, which demonstrate that when $u_k\to 1$, we have $\sin\gamma\to 0$, this results in $R_c\to 0$, as shown in the bottom panel.

This example highlights that the mutual inclination between the two orbits is not a crucial factor after the kick. Rather, the orientation of the kick velocity in relation to the star's velocity is more important in determining the outcome of the orbit, particularly when the magnitudes of the two velocities are similar. Larger kick velocities, such as in the case when the spins are misaligned with respect to the BH binary's angular momentum, yield more unbound systems.

In the bottom row of Figure 2, we compare R_c to the tidal radius (top dashed line):

$$r_{\rm circ} \sim 2R_{\star} \left(\frac{M_{\rm new}}{m_{\star}}\right)^{1/3},$$
 (8)

and to the Roche radius (bottom dashed line):

$$r_{\text{Roche}} \sim R_{\star} \left(\frac{M_{\text{new}}}{m_{\star}}\right)^{1/3}$$
 (9)

A BH approaching the star inside either of these limits will likely result in an EM source. Orbits with $R_c \lesssim r_{\text{Roche}}$ will result in the tidal disruption of the star (or, in some cases, a

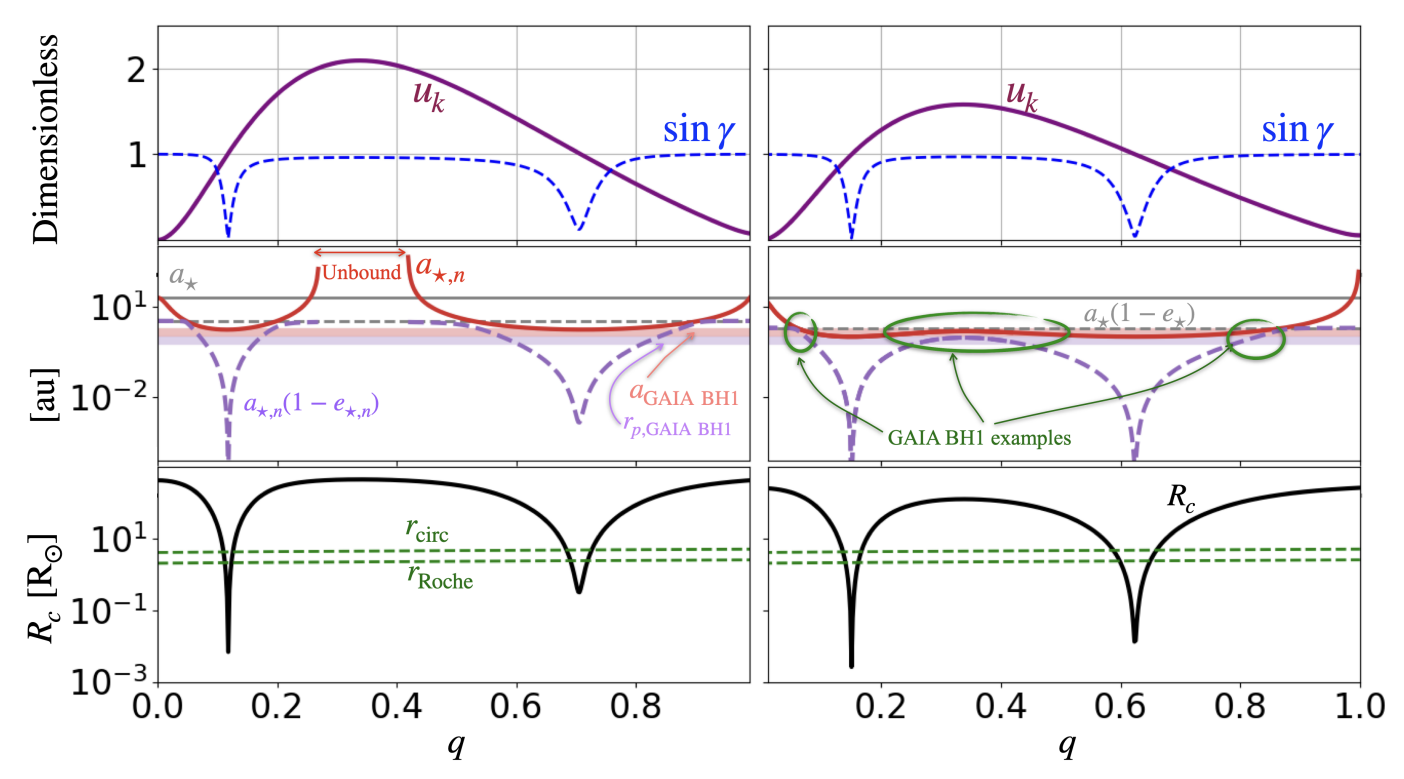


Figure 2. Two examples of the orbital outcome of a recoil kick on an orbit. We consider a system of two low-spin BHs with $S_1 = S_2 = 0.01$ and spin-orbit angles of 2° , 1° , $\Omega_{s1} = 90^{\circ}$, and $\Omega_{s2} = 270^{\circ}$. The mutual inclination is set to 0.1. Before the kick, the star has a semimajor axis of 20 au and eccentricity $e_{\star} = 0.9$ (right column), and $e_{\star} = 0.83$ (left column). The argument of periapsis of the inner (outer) binary at the time of the merger is 300° (20°). These angles are relevant for the rotation of the various vectors to the invariant plane. See the text for more details. We assume that the kick took place when the star's phase was at 10° (right column) and 5° (left column). Various post-merger quantities are shown as a function of the mass ratio of the two original BHs, q. The bottom row shows the closest approach, Equation (3). Overplotted are the tidal radius, r_{circ} , and the Roche radius, r_{Roche} . We expect EM signatures for BHs that approach their stellar companion within these radii. The middle row depicts the post-kick semimajor axis $a_{\star,n}$, with the solid red lines, and the pericenter $a_{\star,n}(1-e_{\star,n})$, with the dashed purple lines. Overplotted are the initial (pre-kick) semimajor axis and pericenter of the star, shown with the solid and dashed gray lines, respectively. Last, Gaia BH1's semimajor axis and pericenter ($a_{\text{Gaia BH1}}$ and $r_{p,\text{Gaia BH1}} = a_{\text{Gaia BH1}}(1-e_{\text{Gaia BH1}})$) are also overplotted, shown with the pink and light purple lines (K. El-Badry et al. 2023b). The top row shows the normalized velocity $u_k = v_{\text{kick}}/v_r$ and $\sin \gamma$, where γ is the angle between the radius vector and the post-kick velocity vector. The grid highlights that when $u_k = 1$, $\gamma \to 0^{\circ}$, thus $R_c \to 0$. Note that here a lower (higher) pre-kick eccentricity, while keeping all of the other parameters constant, yields a wider, more easily unbound (tighter) post-kick binary. The opposite trend is expected for a kic

direct collision; e.g., H. B. Perets et al. 2016; G. Fragione & N. Leigh 2018; S. C. Rose et al. 2022; T. Ryu et al. 2022, 2023, 2024; Y. Yang et al. 2022; C. Xin et al. 2024). Orbits with $r_{
m Roche} \lesssim R_c \lesssim r_{
m circ}$ will lead to the orbit circularizing by tides, eventually producing a mass-transferring system, such as a low-mass X-ray binary (LMXB). We discuss these outcomes in more detail below. Note that $r_{\rm circ}$ is related to the tidal capture radius (W. H. Press & S. A. Teukolsky 1977), but in our case, most of the post-BH merger orbits are already bound, so there is no "capture." The relevant radius is instead the pericenter distance, inside which tides lead to circularization on a timescale less than the evolutionary time of the star. This is likely a factor of a few larger than the traditional tidal capture radius used in Equation (8) (see, e.g., Y. Wu 2018), so our estimates of the fraction of the stars producing XRBs are likely conservative.

The orbital configuration of the bound binary can be estimated by assuming that the kick is instantaneous (e.g., V. Kalogera 2000):

$$\frac{a_{\star,n}}{a_{\star,0}} = \frac{\beta(1 - e_1 \cos E_{\star})}{2\beta - (1 + e_{\star} \cos E_{\star})(1 + u_{\iota}^2 - 2u_{\iota} \cos \theta)}, \quad (10)$$

with

$$\beta = \frac{m_1 \star + M_n}{m_+ + M},\tag{11}$$

where the normalized velocity and the angle θ are defined above. The post-kick semimajor axis can shrink (expand) if β is larger (smaller) than $\beta > 1 + u_k^2 - 2u_k \cos \theta$ (C. X. Lu & S. Naoz 2019). The post-kick BH-stellar orbital eccentricity is given by (C. X. Lu & S. Naoz 2019)

$$e_{\star,n}^2 = 1 - \frac{|\mathbf{r} \times (\mathbf{v}_r + \mathbf{v}_{\text{kick}})|^2}{a_{\star,n}G(m_{\star} + M_{\text{new}})}.$$
 (12)

Note that v_{kick} is calculated in the plane of the inner binary, while v_r is defined in the plane of the outer orbit. We thus rotate all vectors to the invariable plane, defined such that the z-axis is parallel to the total angular momentum. We use the pre-kick relevant angles. Specifically, the relevant angles are the angles between each orbit's angular momenta and the total angular momentum, i_1 and i_2 , for the inner and outer orbits, respectively, and the arguments of periapsis of the inner and outer orbits. In such a frame of reference, the difference between the inner and outer longitude of ascending nodes is π (e.g., S. Naoz et al. 2013a).

Figure 2 illustrates the post-kick semimajor axis and eccentricity of the previously discussed example systems, comparing them to their pre-kick values (see the labels). The left side shows an example where part of the parameter space resulted in the system becoming unbound. In contrast, the right column presents a scenario in which a newly formed BH and the star remained bound, leading to a contraction of the post-kick semimajor axis across a broad range of the parameter space. Overlaid on the figure are the Gaia BH1 orbital parameters from K. El-Badry et al. (2023b). This example demonstrates that such processes can naturally lead to the formation of a Gaia BH1 configuration, as well as other configurations of bound systems.

3. A Population Study

As a proof of concept, we focus on a population of isolated BH binaries that will ultimately become LVK sources and add a stellar tertiary to them. The isolated binary channel involves a common-envelope, stable-mass-transfer phase or chemically homogeneous evolution (e.g., K. Belczynski et al. 2002, 2007; M. Dominik et al. 2012, 2015; S. E. de Mink & I. Mandel 2016; I. Mandel & S. E. de Mink 2016; S. Stevenson et al. 2017; M. Gallegos-Garcia et al. 2021). We thus adopt binary BH orbital configurations that isolated binary population synthesis work suggests will merge. Specifically, we are motivated by the angular momentum constraints from Figure 13 in M. U. Kruckow et al. (2018), which represents the orbital configurations of two BHs, right after the formation of the second BH. Specifically, we choose the initial BH binary eccentricity from a uniform distribution between 0 and 1 and apply the angular momentum constraints on the binary's semimajor axis. Additionally, the population is limited to a merger time of ≤10 Gyr (which reduces the population by a factor of 2). Note that an eccentric BH binary torques the star's inclination via the inverse eccentric Kozai Lidov (iEKL) mechanism; at the time of merger, the BH binary dissipates its eccentricity via GW emission.

For simplicity, the BH masses are adopted from a uniform distribution, each between 9 and $100\,M_\odot$. We note that the choice of mass distributions here may affect the resulting rates at the order of $\sim \pm 10\%$ –20%, as tested via toy models adopting a double power law, with Gaussian peaks for the LVK mass distribution, following T. A. Callister & W. M. Farr (2024) and The LIGO Scientific Collaboration et al. (2025). These tests are omitted here, to avoid clutter. Given these and other uncertainties, we reserve a more detailed analysis for future endeavors.

For the outer orbit, we are motivated by triple conditions that include post-main-sequence stellar evolution for massive stars (e.g., S. Naoz et al. 2016; A. P. Stephan et al. 2019; A. Vigna-Gómez et al. 2021; F. Kummer et al. 2025; C. Shariat et al. 2025b). We thus choose the star's semimajor axis⁸ from a log-normal distribution between [3–100] au and a thermal distribution for the eccentricity (e.g., C. Shariat et al. 2025a). Note that this approach assumes zero (or very small) BH natal velocity (e.g., S. Naoz et al. 2016; C. Shariat et al. 2025b). Last, the mutual inclination between the inner and outer binary is chosen from an isotropic distribution (uniform

in $\cos i$); the arguments of the inner and outer perihelions are chosen from a uniform distribution from 0 to 2π .

The setup of the system is such that in most parts of the parameter space, the BH binary torques the star rather than the star influencing the dynamics of the BH binary. This can yield a preferred orientation for the star's orbital plane (e.g., S. Naoz et al. 2017; B. M. S. Hansen & S. Naoz 2020). To find the possible effect of the star's orientation, we solve the hierarchical triple-body equation of motion up to the hexadecapole level of approximation. There are two main reasons for the usefulness of this approximation beyond the octupole level. The first is that it allows us to integrate inner binaries with comparable masses. The second reason relates to the fact that in some of the systems, the ratio between the period of the outer orbit and the timescale of the quadrupole-level EKL cycles is comparable to or larger than the strength of the octupole term. It has been demonstrated that in such systems, the octupole level is insufficient, and the next-level approximation, i.e., hexadecapole, allows for a more accurate description of the dynamics (e.g., S. Soderhjelm 1975; M. Ćuk & J. A. Burns 2004; L. Luo et al. 2016; C. M. Will 2017, 2021; S. Tremaine 2023; Y. Y. Klein & B. Katz 2024). Additionally, we include the first post-Newtonian (1PN) precession of the inner and outer orbit, which can either suppress or excite eccentricity oscillations for either orbit (e.g., S. Naoz et al. 2013b, 2017; C. M. Will 2017; H. Lim & C. L. Rodriguez 2020). We neglect the 1.5PN and 2PN terms, which would slow down the calculation and only impact spin evolution and not significantly change the orbital precession. On the other hand, we add the 2.5PN terms, which induce orbital shrinking and circularization via GW emission according to, e.g., P. C. Peters & J. Mathews (1963) and P. C. Peters (1964).

The initial conditions, as well as all systems throughout their evolution, satisfy the dynamical stability requirement:

$$\epsilon = \frac{a_{\rm BH}}{a_{\star}} \frac{e_{\star}}{1 - e_{\star}^2} \leqslant 0.1,\tag{13}$$

where ϵ is the dimensionless parameter that appears as the prefactor of the octupole-level term in the hierarchical three-body Hamiltonian (e.g., Y. Lithwick & S. Naoz 2011; S. Naoz et al. 2013a). Although various alternative stability criteria exist in the literature (e.g., R. A. Mardling 2010; J. Mushkin & B. Katz 2020; M. Tory et al. 2022; P. Vynatheya et al. 2022; E. Zhang et al. 2023), the ϵ criterion has been shown to be broadly consistent with many of these (e.g., S. Naoz & D. C. Fabrycky 2014). Furthermore, while the inclusion of higher-order terms, such as the hexadecapole-level approximation, can extend the validity of secular dynamics to more compact systems (e.g., C. M. Will 2017), the $\epsilon \leq 0.1$ threshold remains a conservative and robust choice.

Since each binary BH is chosen such that it will merge within 10 Gyr, we explore the orbital configuration of the stellar tertiary in random intervals. Specifically, we sample the system 1000 times during the integration lifetime. The latter is set to explore the full dynamical extent of the system. Because the mass of the star is small compared to that of the inner binary, the inner binary can also torque the star, known as the iEKL mechanism (e.g., S. Naoz et al. 2017, 2020; M. Zanardi et al. 2017; B. R. Vinson & E. Chiang 2018). For the entire population, we find that the iEKL quadrupole-level timescale for the population is much longer than the quadrupole-level

Note that the aforementioned studies yield wide tertiary orbital separations. Tighter configurations may increase the rates of the various outcomes.

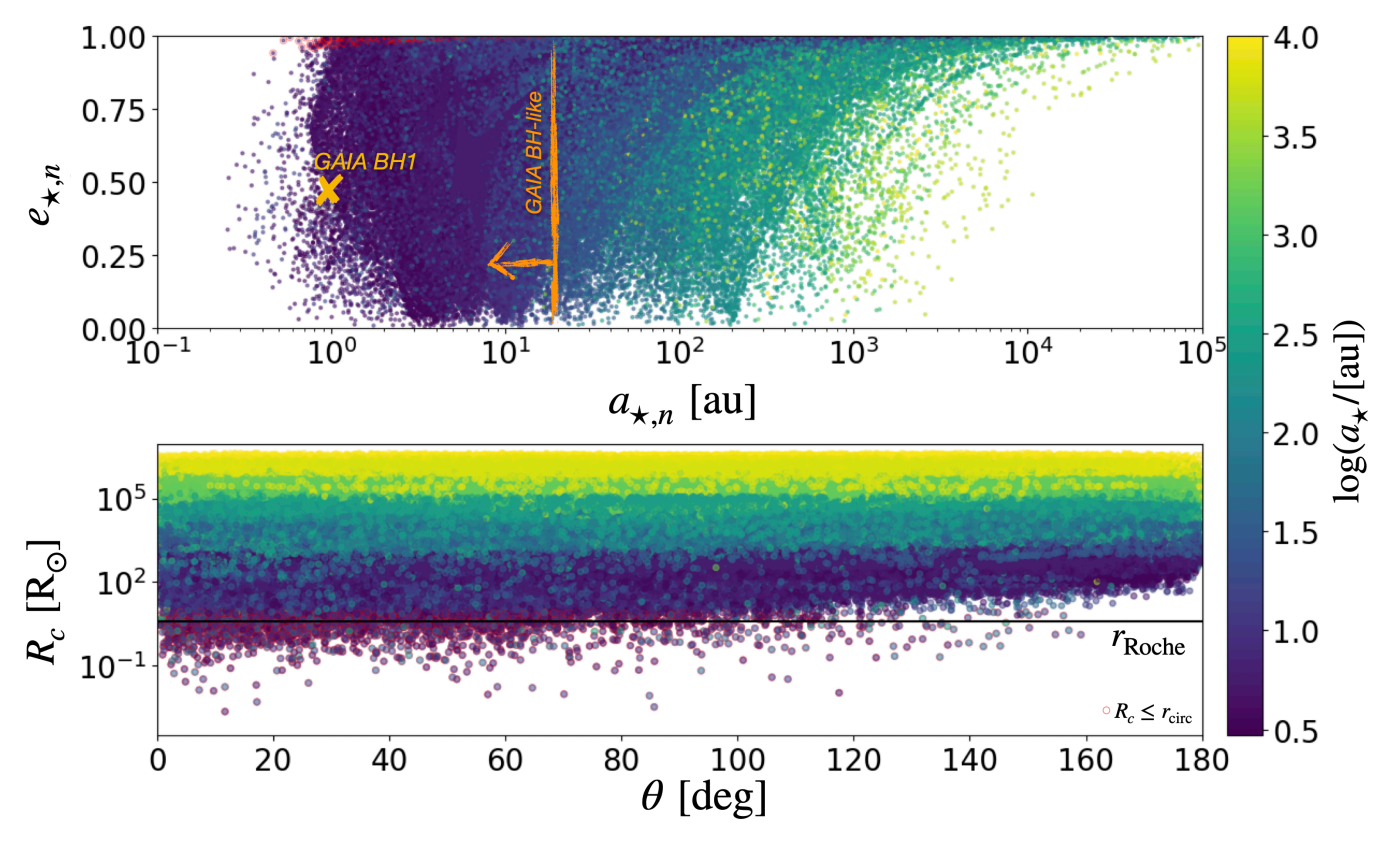


Figure 3. Post-kick orbital configurations of the proof-of-concept population. The top panel presents the post-kick bound population (13% of all systems) and shows the eccentricity (y-axis) and semimajor axes (x-axis) of the star-BH orbits. Overplotted are the orbital parameters of Gaia BH1 (e.g., K. El-Badry et al. 2023b) and the approximate part of the parameter space potentially detectable by Gaia (defined by having a period up to 10 yr and pericenter larger than $r_{\rm circ}$). The bottom panel shows the closest approach (which is the pericenter for bound systems) of all of the systems in the simulation as a function of the angle between the recoil kick vector and the star's initial (pre-kick) orbital velocity, i.e., $\theta = v_r \cdot v_{\rm kick}/(v_r v_{\rm kick})$. Overplotted is the Roche radius. The color code depicts the star's initial (pre-kick) semimajor axis. The points with red edges are those that have $R_c \leqslant r_{\rm circ}$ and are therefore likely to produce EM emission.

timescale to torque the inner binary, i.e.,

$$t_{\text{quad}} \sim \frac{16}{15} \frac{a_{\star}^3 (1 - e_{\star}^2)^{3/2} \sqrt{m_1 + m_2}}{a_{\text{BH}}^{3/2} m_{\star} \sqrt{G}}.$$
 (14)

Thus, to allow sufficient simulation time for either the BH binary or the stellar orbital parameters to evolve dynamically, we adopt the descent timescale, $t_{\rm descent}$. This quantity describes the time required to reach extreme eccentricity via higher-order approximations of the Hamiltonian. Recently, G. C. Weldon et al. (2024) found an analytical expression for this timescale, i.e.,

$$t_{\text{descent}} = t_{\text{quad}} + \Upsilon t_{\text{oct}} \eta(r_{p,\text{min}}),$$
 (15)

where t_{quad} is defined in Equation (14) and

$$t_{\text{oct}} = \frac{64}{15} G^{-1/2} \frac{a_{\star}^4}{a_{\text{BH}}^{5/2}} \frac{(m_1 + m_2)^{3/2}}{(m_1 - m_2)m_{\star}} \frac{(1 - e_{\star}^2)^{5/2}}{e_{\star}}.$$
 (16)

We thus integrate each system to $t_{\rm age} = \min(t_{\rm descent}, 1 \, {\rm Gyr})$ or until the inner binary merges. We discarded systems that became unstable during the evolution (2% of all systems), because the secular equations do not describe the full dynamics for these systems (e.g., S. Naoz et al. 2017).

Last, at each output time step, we adopt an eccentric anomaly for the star chosen from a uniform distribution. The spins of the BHs remain aligned with $i_{s1} = 2^{\circ}$ and $i_{s2} = 2^{\circ}$, and Ω_{s1} and Ω_{s1} are chosen from a uniform distribution.

Figure 3 depicts the results of this proof-of-concept population study. The top panel shows the post-kick bound systems' semimajor axes and eccentricity (representing 13% of the systems). The bottom panel shows the closest approach of all systems as a function of the angle θ , which is the angle between the recoil kick velocity and the star's velocity vector just before the kick took place. The red circles indicate systems that have a closest approach (pericenter in the case of bound systems) smaller than $r_{\rm circ}$, from Equation (8). The color code represents the star's initial semimajor axis.

As demonstrated in this example, Gaia-BH-like systems naturally form post-kick, and they happen for systems with typical initial semimajor axes of \sim 12 au. However, there is a long tail of initial separations that can produce Gaia-BH-like systems, with the widest one being \sim 6 × 10³ au. Moreover, this channel produces a wide range of detached BH-star systems, reaching up to 10⁴ au in separation.

The initial separation of the star is a key factor in determining the post-kick configuration, both for Gaia-BH-like systems and for those with $R_c \lesssim r_{\rm circ}$. As highlighted in the bottom panel of Figure 3, very wide ($\sim 10^4$ au) pre-kick stars are less likely to end up with a small R_c . Specifically, those that cross $r_{\rm circ}$ have, on average, a pre-kick semimajor axis of 13 au, but again with a long tail extending up to $a_{\star} \sim 10^3$ au.

4. Rates and Detectability

4.1. General Considerations

Rate estimates involve considerable uncertainty and should therefore be taken with a grain of salt. Here, we aim to estimate the order-of-magnitude contribution of this channel to EM signatures and Gaia-BH-like systems. We begin by assuming that the BH binaries produced by triples as modeled here are representative of LVK detections, with a rate estimated as $\Gamma_{LVK} \sim 30\, \text{Gpc}^{-3}\, \text{yr}^{-1}$ (e.g., R. Abbott et al. 2023). We note that there are many different proposed channels for LVK mergers, and that this assumption by itself is very strong. Other ideas in the literature suggest that dynamical scattering in globular clusters can produce a significant fraction of LVK sources (e.g., C. L. Rodriguez et al. 2016, 2018; J. Samsing 2018), as well as other dynamical channels, such as in galactic nuclei (e.g., R. M. O'Leary et al. 2009; C. Petrovich & F. Antonini 2017; B.-M. Hoang et al. 2018), fly-by interactions in the field (e.g., E. Michaely & H. B. Perets 2020), hierarchical triples (e.g., K. Silsbee & S. Tremaine 2017; F. Kummer et al. 2025), or active galactic nucleus (AGN) disks (e.g., H. Tagawa et al. 2020; J. Samsing et al. 2022). Regardless, the isolated binary channel is likely to also be significant (e.g., P. Nutzman et al. 2004; K. Belczynski et al. 2016; K. Breivik et al. 2016; S. E. de Mink & I. Mandel 2016; I. Mandel & S. E. de Mink 2016; P. Marchant et al. 2016). Therefore, the rate below can be normalized by the contribution of field binaries to LVK sources.

Taking the field binaries as the main contributions, we remind the reader that our initial condition setup of the binary, as described in Section 3, represents about 50% of the BH orbital configuration that will lead to mergers. In other words, $f_{\rm BH} \sim 0.5$. Note that we start with the LVK merger sample, but half of the mergers take too long for the tertiary $1 M_{\odot}$ star to still be around. Notably, about 70% of massive binaries are in a triple configuration (e.g., M. Moe & R. Di Stefano 2017; S. S. R. Offner et al. 2023). However, since ∼solar-mass companions can be missed, this is may be a lower limit, and we assume for simplicity that all massive binaries have a tertiary. 10 Furthermore, the fraction of these triples hosting a $\sim 1 \, M_{\odot}$ star is $f_1 \sim 0.2$, estimated from the tertiary mass ratio distributions in triples in C. Shariat et al. (2025a). While a more massive tertiary would increase the predicted fractions, its shorter main-sequence lifetime could limit the time available for this process to occur. A detailed study of the tertiary IMF is left for future work.

With these two fractions, we can proceed to estimate the probabilities of the different outcomes, as well as their EM detectability.

4.2. EM Signatures

Here, we divide the discussion into systems that crossed the tidal radius $r_{\rm circ}$ ($f_{\rm capt} \sim 0.002$ out of all systems) and the $\sim 50\%$ of that subset that also crossed the Roche radius, so the

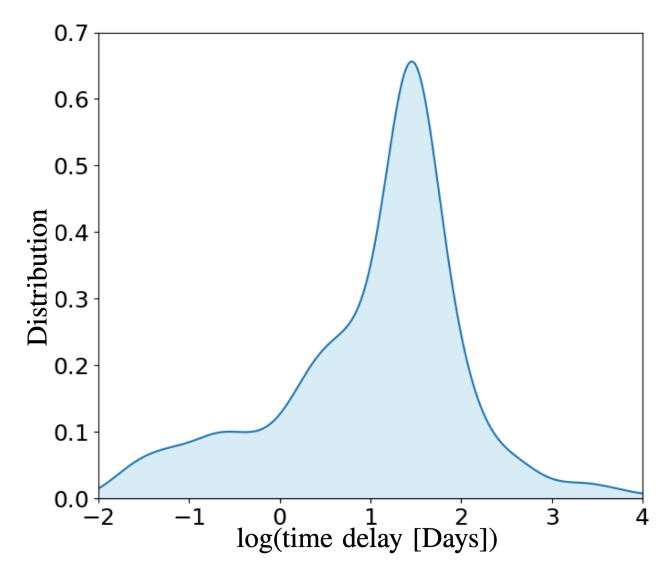


Figure 4. Time-delay distribution for the EM counterpart, assumed to be the time between the merger of the inner BH binary and when the BH remnant–star separation shrinks below $r_{\rm circ}$. Both bound (87% of all systems with $R_c \leqslant r_{\rm circ}$) and unbound systems, as well as those that crossed the star's Roche limit (\sim 50% out of all systems with $R_c \leqslant r_{\rm circ}$), exhibit the same distribution. The average of this distribution is \sim 10 days. We note that the fallback time of the bound debris onto the BH is on the order of a day or less; see Equation (19).

star is disrupted. Therefore, we find:

$$\Gamma_{\rm capt} \sim \Gamma_{\rm LV\,K} \times f_{\rm BH} \times f_1 \times f_{\rm capt} \sim 0.006~{\rm Gpc^{-3}~yr^{-1}}, \quad (17)$$

$$\Gamma_{\rm Roche} \sim \Gamma_{\rm LV\,K} \times f_{\rm BH} \times f_1 \times \frac{f_{\rm capt}}{2} \sim 0.003 \ {\rm Gpc^{-3} \ yr^{-1}}.$$
 (18)

Since no reliable EM signature has been observed so far in LVK (e.g., N. Veronesi et al. 2025), naturally we expect a less than 1% event rate, which agrees with the above estimates. Specifically, 0.02% (0.01%) of LVK BH binary mergers may be accompanied by EM counterparts, crossing $r_{\rm circ}$ ($R_{\rm Roche}$). If the future LVK campaigns O5 or O6 yield more than a total of 5000 events, we predict the possible detection of an EM counterpart associated with a BH merger.

An important question to consider is: what is the time delay between a GW event and the crossing of $r_{\rm circ}$ and $R_{\rm Roche}$? In the triple scenario considered here, this is a lower limit on the time delay between an EM counterpart and the binary BH merger that preceded it. Figure 4 illustrates the distribution of time delays, indicating an average delay of about 10 days between the merger and its EM counterpart. All possible combinations of outcomes, whether the tertiary star is bound or unbound, and whether it crosses $r_{\rm circ}$ or $R_{\rm Roche}$, exhibit the same distribution.

There are two distinct classes of EM sources that our scenario can produce. Stars with $R_c \lesssim r_{\rm Roche}$ will undergo tidal disruption with a bright, relatively prompt EM flare, delayed relative to the GW event by the amount shown in Figure 4. By contrast, stars with $r_{\rm Roche} \lesssim R_c \lesssim r_{\rm circ}$ will slowly circularize by tides and eventually produce a mass-transferring binary, resembling a long-lived Galactic XRB more than a prompt EM flare. The time delay between the GW event and the onset of EM emission from mass transfer will typically be set by the stellar evolution timescale of the tertiary and so will be of the order of Gyr. In this case, it will of course not be possible to

⁹ As mentioned in Section 3, we select a BH binary population with a merger timescale shorter than 10 Gyr, which is effectively half of the population synthesis considered by M. U. Kruckow et al. (2018).

synthesis considered by M. U. Kruckow et al. (2018).

Note that the fraction of surviving BH binaries with tertiaries remains uncertain. Specifically, while the observational constraints on unbound tertiaries to supernova counterparts are low (e.g., K. Barboza & C. S. Kochanek 2024), the connection between these systems and LVK sources is yet to be established.

temporally correlate the GW and EM signals, and the EM signal is likely to be far too faint to detect beyond nearby galaxies (i.e., individual XRBs cannot be seen at cosmological distances). We thus focus our discussion here on the regime of $R_c \lesssim r_{\rm Roche}$, which has the potential to produce a prompt detectable EM counterpart to the cosmological binary BH mergers detected in GWs (e.g., H. B. Perets et al. 2016; G. Fragione & N. Leigh 2018; Y. Yang et al. 2022; C. Xin et al. 2024).

In the regime $R_c \lesssim r_{\rm Roche}$, the primary outcome is an EM flare associated with the tidal disruption of the star by the newly formed BH. The fallback timescale, the time it takes the bound debris of the disrupted star to fall back onto the BH, is given roughly by

$$t_{\rm FB} \approx 2\pi \frac{r_{\rm Roche}^3}{r_{\star}^{3/2}} \frac{1}{\sqrt{GM_{\rm new}}} = 4\pi \frac{r_{\star}^{3/2}}{m_{\star}} \sqrt{\frac{M_{\rm new}}{G}},$$

$$\approx 1.6 \, \text{days} \left(\frac{r_{\star}}{R_{\odot}}\right)^{3/2} \left(\frac{m_{\star}}{M_{\odot}}\right)^{-1} \left(\frac{M_{\rm new}}{50 \, M_{\odot}}\right)^{1/2}. \tag{19}$$

E. R. Coughlin & C. J. Nixon (2022) and A. Bandopadhyay et al. (2024) found that, for disruptions around a supermassive BH, the fallback time may be shorter by an order of magnitude than this estimate, with little dependence on stellar mass for a main-sequence star. Therefore, Equation (19) is likely an upper limit on the fallback time. Equation (19) thus shows that the bound debris of the disrupted star will fall back onto the BH within a day or so—much shorter than the time delay in Figure 4 set by the time it takes the star and BH to interact after the GW merger. The delay between the GW source and its EM counterpart will thus largely be set by the timescale given in Figure 4.

Observations of tidal disruption events (TDEs) by supermassive BHs show a rich phenomenology across the EM spectrum. A small fraction of sources show bright nonthermal X-ray and gamma-ray emission associated with a relativistic jet, but such prominent jet emission is much rarer in TDEs than in AGNs or XRBs (S. Komossa et al. 2003). Instead, the dominant signature of TDEs is thermal optical—UV—X-ray emission and radio emission produced by outflows interacting with the interstellar medium (S. Gezari 2021; Y. Cendes et al. 2024).

The key difference between the TDEs by solar-mass BHs considered here and those associated with supermassive BHs is that the shorter fallback time and lower BH mass imply that the fallback rate is highly super-Eddington. This is likely to suppress bright high-energy emission from the vicinity of the BH, because it is enshrouded in the optically thick super-Eddington envelope (except perhaps for very favorable viewing angles down the spin axis of the system or if a jet escapes the optically thick envelope). In this case, the most likely robust EM counterpart is a thermal optical-UV flare powered by the super-Eddington outflow, with luminosities of up to $\sim \! 10^{44}$ erg s⁻¹ and durations of days to weeks (e.g., K. Kremer et al. 2019, 2021). The sources will likely resemble the optical-UV emission in fast blue optical transients, such as 2018cow (R. Margutti et al. 2019; D. A. Perley et al. 2019), which are also interpreted as TDEs or mergers between stars and stellar-mass compact objects or intermediate-mass BHs (B. D. Metzger 2022; I. Linial & E. Quataert 2024; D. Tsuna & W. Lu 2025).

In a fraction of the TDE cases considered here with $r_{\rm Roche} \lesssim R_c \lesssim 2r_{\rm Roche}$, the star will only be partially disrupted at pericenter, likely leading to a periodic optical–UV transient with a period of about 2 months (set by Figure 4); this is analogous to the partial tidal disruption candidates by supermassive BHs observed in galactic nuclei (e.g., A. V. Payne et al. 2021).

Finally, we note that during the red-giant phase, the probability of tidal disruption is significantly higher, because of the larger stellar radius. However, a solar-mass star only spends $\sim 1\%$ of its lifetime with a radius $\gtrsim 10R_{\odot}$, so the redgiant phase likely does not enhance the overall rate of EM counterparts significantly. The fallback time for red giants will also be longer (Equation (19)), leading to a longer delay between the EM and GW sources and likely a fainter EM counterpart, because of the lower fallback rates.

4.3. Gaia-BH-like Systems

To estimate the efficiency of this channel in producing Gaia-BH-like systems, we begin by estimating the total number of LVK sources in a galaxy, assuming that galaxies with masses comparable to the Milky Way (MW) produce a significant fraction of the LVK rate (if they do not, the estimates below of Gaia-BH-like systems in the MW are upper limits). We note that the LVK binaries are often thought to have originated from a low-metallicity environment (e.g., M. Dominik et al. 2012; C. L. Rodriguez et al. 2015; M. Fishbach & V. Kalogera 2021). However, the strong metallicity dependence of BH binary formation is still uncertain (e.g., L. A. C. van Son et al. 2025). Thus, estimating the galactic BHs from LVK mergers is done here just to provide an order-of-magnitude sense of the number of galactic BHs where post-merger recoil could be important for setting the system properties.

Given the number densities of massive galaxies ~ 0.01 – $0.001~\rm Mpc^{-3}$ (e.g., C. J. Conselice et al. 2016), over a Hubble time, the expected number of BH mergers per galaxy is $N_{\rm BBH} \sim 3 \times 10^{4-5}$. Thus, to estimate the number of Gaialike systems, we multiply this number by $f_{\rm BH} \times f_{1}$ —i.e., the fraction that our initial conditions represent from the total simulated binary BH population. Then, we multiply this by $f_{R_{\rm s}10} \sim 0.08$, which is the fraction of systems out of all runs that remain bound after the kick, have a period smaller than 10 yr, and have a pericenter larger than $r_{\rm circ}$. Thus, the expected Gaia BH candidates from this channel are

$$N_{\text{Gaia-BH}} \sim N_{\text{BBH}} \times f_{\text{BH}} \times f_1 \times f_{P_{\leq 10}} \sim 240 - 2400.$$
 (20)

The total number of Gaia-BH-like systems in our MW is estimated to be about 20,000 (P. Nagarajan et al. 2025), thus this channel may contribute to 1%-10% of Gaia-BH-like systems. In our models, these Gaia-BH-like populations have an average separation of \sim 7 au and eccentricity of 0.6. This estimate does not depend on the spin of the BHs, but it is sensitive to the alignment of the BHs, where misaligned BHs will result in even fewer post-kick bound systems. A small misalignment for the less (more) massive BH $\lesssim 10^{\circ}$ (5°) has a negligible effect on the results. While the binary merger channel naturally results in spin alignment, in some cases, where the star is on a tight orbit, it torques the inner BH binary orbit, which may result in misalignment (e.g., B. Liu & D. Lai 2018). We reserve this part of the investigation for future work.

Overall, we estimate that about 13% of all systems remain bound, with an average separation of \sim 594 au and eccentricity of 0.6. Of these, about 60% have a period of less than 10 yr, yielding a Gaia-BH-like system. The remaining \sim 40% are wider detached BH-star binaries.

5. Conclusion and Discussion

The detection of stellar-mass BHs through EM signatures (e.g., XRBs), GWs from merging binaries, and astrometric measurements of wide-orbit companions (Gaia BHs) has revealed a diverse population of systems. While each observational method probes a range of different physical processes and possibly stages in the life of a BH, connecting these distinct populations has remained an open challenge.

Here, we propose a new formation channel that naturally bridges these populations. By focusing on massive stellar triples, which constitute the majority of massive star systems (e.g., M. Moe & R. Di Stefano 2017), we show that the merger of an inner BH binary, followed by the resulting recoil kick, can lead to four distinct outcomes:

- (1) A prompt transient EM counterpart to the GW merger, due to the tidal disruption of the star by the BH and subsequent highly super-Eddington accretion. The transient will occur about 10 days after the BH merger (Figure 4) and will likely be a bright optical—UV flare lasting a few days to a week, in some ways analogous to luminous fast blue optical transients. In a subset of cases, the transient will be a partial tidal disruption leading to a repeating EM counterpart with a period of order 2 months;
- (2) A BH-stellar system that slowly circularizes due to tidal interaction, eventually undergoing mass transfer and producing an LMXB (likely Gyr after the GW merger);
- (3) A wide BH-stellar companion system, akin to Gaia BHs; or
 - (4) An unbound system (i.e., a single isolated BH).

These outcomes are illustrated schematically in Figure 1 and through examples in Figure 2. An important feature of our model to stress is that the tertiary companion is not dynamically important in the evolution of the inner binary. Instead, we have explored the outcome of a passive tertiary in an otherwise binary-driven BH merger channel.

To explore this scenario, we performed a proof-of-concept population study of BH binaries with a $1\,M_\odot$ tertiary companion, motivated by the isolated binary BH merger channel (e.g., K. Belczynski et al. 2002, 2007). In this initial exploration, we fixed the tertiary mass and found that the final configuration depends most strongly on the star's initial orbital separation, rather than other orbital parameters, such as mutual inclination. Specifically, while counterintuitive, the mutual inclination does not play a key role, because the new BH-star binary relative velocity is a combination of the kick and the pre-kick velocity. As expected, wider-orbit stars are more likely to become unbound. Among systems that ended up in a close post-kick encounter (crossing the tidal radius), the pre-kick separation averaged ~ 13 au, with a wide tail extending up to $\sim 10^3$ au.

In this proof-of-concept analysis, we adopted negligible BH natal kicks. However, various theoretical supernova models predict significant mass ejection for BH progenitors across a wide range of parameters, yielding a wide range of kick velocities (e.g., C. L. Fryer et al. 2012; S. Repetto et al. 2012;

B. Müller et al. 2016; I. Mandel & B. Müller 2020; K. Maltsev et al. 2025). These kicks, along with the mass loss that occurs suddenly during BH formation (e.g., A. Blaauw 1961; J. G. Hills 1983), can impact the configuration of triple systems and may even lead to the unbinding of the system. For instance, it has been suggested that such kicks could reduce the BH merger rate by a factor of a few (e.g., F. Antonini et al. 2017; K. Silsbee & S. Tremaine 2017). On the other hand, some recent observational systems, including VFTS 243 and V404 Cygni, indicate negligible BH natal kicks (e.g., T. Shenar et al. 2022; K. B. Burdge et al. 2024; A. Vigna-Gómez et al. 2024, 2025; C. Shariat et al. 2025b; R. Willcox et al. 2025). Nonetheless, the uncertainty surrounding these estimates is considerable, and we caution that the rates discussed in this Letter may have substantial uncertainties. The full evolution of triple stars during their lifetime, including BH natal kicks, is reserved for future studies.

A key factor governing the outcome is the angle θ between the star's pre-kick velocity vector and the kick direction. When the kick velocity is comparable to the stellar orbital speed, where the vectors are aligned, this is more likely to result in a small impact parameter and, thus, close approaches. This follows from Equation (3), which shows that close encounters require small impact parameters relative to $G(m_{\star} + M_{\rm new})/v_{\rm new}^2$. Since eccentric companions spend most of their orbit near apocenter, close approaches typically occur when the kick velocity nearly cancels the orbital motion (see Section 2.2 and the bottom panel of Figure 3). For the parameter choices adopted here, we estimate that \sim 0.02% of LVK sources may be followed by an EM counterpart, with a short time delay (averaging around 10 days; see Figure 4).

Interestingly, about 13% of our sample resulted in a bound star-BH configuration after the kick. Notably, $\sim 8\%$ of the sample formed systems with post-kick orbital periods less than 10 yr, comparable to the Gaia BH candidates. Our channel can resolve the difficulty of producing systems like Gaia BH1, where the stellar companion currently resides at a separation that would have been engulfed during the BH progenitor's redgiant phase. This tension has led to several proposed explanations, including fine-tuned mass transfer or envelope ejection, triple-star evolution, and natal BH kicks that reshaped the orbit (e.g., K. El-Badry et al. 2023b; A. Generozov & H. B. Perets 2024; Z. Li et al. 2024; M. Fishbach et al. 2025). While the natal kick explanation shares features with the mechanism we propose, recent detections of XRBs with tertiary companions suggest that at least some BHs may receive small or negligible natal kicks (e.g., K. B. Burdge et al. 2024; C. Shariat et al. 2025b). Our results show that Gaia-BH-like systems can arise naturally following a BH merger and recoil kick, without requiring extreme assumptions about natal kicks. Based on our toy model, we estimate that this channel could contribute between 1% and 10% of all Gaia BHs in the Galaxy.

Crucially, the framework proposed here not only accounts for the GW detections by LVK, but also offers a viable pathway for forming Gaia BHs and, in some cases, XRBs, thereby linking all three observational channels for the first time within a single evolutionary scenario. It also predicts a robust channel for producing EM counterparts to binary BH mergers.

Acknowledgments

We thank the anonymous referee for the useful and detailed report. S.N. acknowledges the partial support of NSF-BSF grant AST-2206428 and NASA XRP grant 80NSSC23K0262, as well as Howard and Astrid Preston for their generous support. Z.H. acknowledges support from NASA grants 80NSSC22K0822 and 80NSSC24K0440. E.Q. thanks the Gordon and Betty Moore Foundation for support through grant GBMF5076.

Appendix GW Recoil Kicks

Here, we provide the fitting formula from C. O. Lousto et al. (2010, 2012) for the post-merger recoil kick. We note that in our case, the velocity is in the plane of the binary. The general kick velocity vector is

$$\mathbf{v}_{\text{kick}} = \mathbf{v}_m \hat{\mathbf{e}} + \mathbf{v}_{\perp} (\cos \xi \hat{\mathbf{e}} + \sin \xi \hat{\mathbf{h}}) + \mathbf{v}_{\parallel} \hat{\mathbf{h}}, \tag{A1}$$

where $\{\hat{e}_{\bullet}, \hat{q}_{\bullet}, \hat{h}_{\bullet}\}$ is the Runge-Lenz coordinate of the BH binary, and \perp and \parallel are components that are perpendicular and parallel, respectively, to the binary's angular momentum, where $\hat{h} = L_{\rm BHs}/L_{\rm BHs}$. Additionally,

$$v_m = A\eta^2 \sqrt{1 - 4\eta} (1 + B\eta), \tag{A2}$$

$$v_{\perp} = \frac{H\eta^2}{1+q} (\chi_{2,\parallel} - q\chi_{1,\parallel}),$$
 (A3)

$$v_{\parallel} = \frac{16\eta^{2}}{1+q} [V_{1,1} + V_{A}\tilde{S}_{\parallel} + V_{B}\tilde{S}_{\parallel}^{2} + V_{C}\tilde{S}_{\parallel}^{3}] \times |S_{2,\perp} - qS_{1,\perp}|\cos(\phi_{\Lambda} - \phi_{1}), \tag{A4}$$

where $\eta = q/(1+q)^2$ is the asymmetric mass ratio, χ_1 and χ_2 are the dimensionless spin vectors, the vector \tilde{S} is defined as

$$\tilde{S} = 2 \, \frac{S_2 + q^2 S_1}{(1+q)^2},\tag{A5}$$

 ϕ_1 is the phase angle of the binary, and ϕ_Δ is the angle between the in-plane component of

$$\Delta = M^2 \frac{\chi_2 - q\chi_1}{1 + a} \tag{A6}$$

and the infall direction at the merger. Following C. O. Lousto et al. (2012), we assume that the angle ($\phi_{\Delta} - \phi_{1}$) is chosen from a uniform distribution [0, 2π) and the constants are: $A=1.2\times 10^4\,\mathrm{km\,s^{-1}}$, $H=6.9\times 10^3\,\mathrm{km\,s^{-1}}$, B=-0.93, $\xi=145^\circ$, $V_{1,1}=3678\,\mathrm{km\,s^{-1}}$, $V_A=2481\,\mathrm{km\,s^{-1}}$, $V_B=1793\,\mathrm{km\,s^{-1}}$, and $V_C=1507\,\mathrm{km\,s^{-1}}$ (J. A. González et al. 2007; C. O. Lousto & Y. Zlochower 2008; C. O. Lousto et al. 2012). This model aligns well with full numerical relativity results, even in the intermediate-mass-ratio regime of $q\sim0.1$ (J. A. González et al. 2009). We also calculate the post-merger mass M_{new} using Equation (4) in C. O. Lousto et al. (2010; omitted here to avoid clutter).

ORCID iDs

Smadar Naoz https://orcid.org/0000-0002-9802-9279 Zoltán Haiman https://orcid.org/0000-0003-3633-5403 Eliot Quataert https://orcid.org/0000-0001-9185-5044 Liz Holzknecht https://orcid.org/0009-0004-0449-8085

References

```
Abbott, B. P., Abbott, R., Abbott, T. D., et al. 2016, PhRvL, 116, 061102
Abbott, R., Abbott, T. D., Acernese, F., et al. 2023, PhRvX, 13, 011048
Agol, E., Kamionkowski, M., Koopmans, L. V. E., & Blandford, R. D. 2002,
   ApJL, 576, L131
Antonini, F., Chatterjee, S., Rodriguez, C. L., et al. 2016, ApJ, 816, 65
Antonini, F., Toonen, S., & Hamers, A. S. 2017, ApJ, 841, 77
Bandopadhyay, A., Fancher, J., Athian, A., et al. 2024, ApJL, 961, L2
Barboza, K., & Kochanek, C. S. 2024, MNRAS, 535, 1315
Belczynski, K., Heger, A., Gladysz, W., et al. 2016, A&A, 594, A97
Belczynski, K., Kalogera, V., & Bulik, T. 2002, ApJ, 572, 407
Belczynski, K., Taam, R. E., Kalogera, V., Rasio, F. A., & Bulik, T. 2007,
    DJ. 662, 504
Blaauw, A. 1961, BAN, 15, 265
Bolton, C. T. 1972, Natur, 235, 271
Breivik, K., Rodriguez, C. L., Larson, S. L., Kalogera, V., & Rasio, F. A.
  2016, ApJL, 830, L18
Burdge, K. B., El-Badry, K., Kara, E., et al. 2024, Natur, 635, 316
Callister, T. A., & Farr, W. M. 2024, PhRvX, 14, 021005
Cendes, Y., Berger, E., Alexander, K. D., et al. 2024, ApJ, 971, 185
Chawla, C., Chatterjee, S., Shah, N., & Breivik, K. 2024, ApJ, 975, 163
Clavel, M., Dubus, G., Casares, J., & Babusiaux, C. 2021, A&A, 645, A72
Conselice, C. J., Wilkinson, A., Duncan, K., & Mortlock, A. 2016, ApJ,
Coughlin, E. R., & Nixon, C. J. 2022, MNRAS, 517, L26
Ćuk, M., & Burns, J. A. 2004, AJ, 128, 2518
de Mink, S. E., & Mandel, I. 2016, MNRAS, 460, 3545
Dominik, M., Belczynski, K., Fryer, C., et al. 2012, ApJ, 759, 52
Dominik, M., Berti, E., O'Shaughnessy, R., et al. 2015, ApJ, 806, 263
Dorozsmai, A., Romero-Shaw, I. M., Vijaykumar, A., et al. 2025, arXiv:2507.
  23212
Dorozsmai, A., Toonen, S., Vigna-Gómez, A., de Mink, S. E., & Kummer, F.
   2024, MNRAS, 527, 9782
El-Badry, K., Rix, H.-W., Cendes, Y., et al. 2023a, MNRAS, 521, 4323
El-Badry, K., Rix, H.-W., Quataert, E., et al. 2023b, MNRAS, 518, 1057
Fishbach, M., Breivik, K., Willcox, R., & van Son, L. A. C. 2025, arXiv:2508.
Fishbach, M., & Kalogera, V. 2021, ApJL, 914, L30
Fishbach, M., & Kalogera, V. 2022, ApJL, 929, L26
Fragione, G., & Leigh, N. 2018, MNRAS, 479, 3181
Fryer, C. L., Belczynski, K., Wiktorowicz, G., et al. 2012, ApJ, 749, 91
Gaia Collaboration, Brown, A. G. A., Vallenari, A., et al. 2021, A&A, 649, A1
Gaia Collaboration, Panuzzo, P., Mazeh, T., et al. 2024, A&A, 686, L2
Gaia Collaboration, Vallenari, A., Brown, A. G. A., et al. 2023, A&A, 674, A1
Gallegos-Garcia, M., Berry, C. P. L., Marchant, P., & Kalogera, V. 2021, ApJ,
  922, 110
Generozov, A., & Perets, H. B. 2024, ApJ, 964, 83
Gezari, S. 2021, ARA&A, 59, 21
González, J. A., Sperhake, U., & Brügmann, B. 2009, PhRvD, 79, 124006
González, J. A., Sperhake, U., Brügmann, B., Hannam, M., & Husa, S. 2007,
  PhRvL, 98, 091101
Graham, M. J., McKernan, B., Ford, K. E. S., et al. 2023, ApJ, 942, 99
Hansen, B. M. S., & Naoz, S. 2020, MNRAS, 499, 1682
Hills, J. G. 1983, ApJ, 267, 322
Hoang, B.-M., Naoz, S., Kocsis, B., Rasio, F. A., & Dosopoulou, F. 2018,
  ApJ, 856, 140
Huang, X., Dodd, S., Schrøder, S. L., Davis, S. W., & Ramirez-Ruiz, E. 2025,
   ApJL, 982, L11
Kalogera, V. 2000, ApJ, 541, 319
Klein, Y. Y., & Katz, B. 2024, MNRAS, 535, L31
Komossa, S., Burwitz, V., Hasinger, G., et al. 2003, ApJL, 582, L15
Kremer, K., Lu, W., Piro, A. L., et al. 2021, ApJ, 911, 104
Kremer, K., Lu, W., Rodriguez, C. L., Lachat, M., & Rasio, F. A. 2019, ApJ,
  881, 75
Kruckow, M. U., Tauris, T. M., Langer, N., Kramer, M., & Izzard, R. G. 2018,
  MNRAS, 481, 1908
Kummer, F., Toonen, S., Dorozsmai, A., Grishin, E., & de Koter, A. 2025,
  A&A, 693, A84
Lam, C. Y., Lu, J. R., Udalski, A., et al. 2022, ApJL, 933, L23
Li, Z., Zhu, C., Lu, X., et al. 2024, ApJL, 975, L8
Lim, H., & Rodriguez, C. L. 2020, PhRvD, 102, 064033
Linial, I., & Quataert, E. 2024, ApJ, 974, 67
Lithwick, Y., & Naoz, S. 2011, ApJ, 742, 94
Liu, B., & Lai, D. 2018, ApJ, 863, 68
Liu, B., Lai, D., & Wang, Y.-H. 2019a, ApJ, 881, 41
Liu, J., Zhang, H., Howard, A. W., et al. 2019b, Natur, 575, 618
```

```
Lousto, C. O., Campanelli, M., Zlochower, Y., & Nakano, H. 2010, CQGra,
   27, 114006
Lousto, C. O., & Zlochower, Y. 2008, PhRvD, 77, 044028
Lousto, C. O., Zlochower, Y., Dotti, M., & Volonteri, M. 2012, PhRvD, 85,
Lu, C. X., & Naoz, S. 2019, MNRAS, 484, 1506
Lu, J. R., Sinukoff, E., Ofek, E. O., Udalski, A., & Kozlowski, S. 2016, ApJ,
   830, 41
Lu, W., Beniamini, P., & Bonnerot, C. 2021, MNRAS, 500, 1817
Luo, L., Katz, B., & Dong, S. 2016, MNRAS, 458, 3060
MacLeod, M., & Grindlay, J. 2023, arXiv:2304.09368
Maltsey, K., Schneider, F. R. N., Mandel, I., et al. 2025, A&A, 700, A20
Mandel, I., & de Mink, S. E. 2016, MNRAS, 458, 2634
Mandel, I., & Müller, B. 2020, MNRAS, 499, 3214
Marchant, P., Langer, N., Podsiadlowski, P., Tauris, T. M., & Moriya, T. J.
   2016, A&A, 588, A50
Mardling, R. A. 2010, MNRAS, 407, 1048
Margutti, R., Metzger, B. D., Chornock, R., et al. 2019, ApJ, 872, 18
Martinez, M. A. S., Rodriguez, C. L., & Fragione, G. 2022, ApJ, 937, 78
Metzger, B. D. 2022, ApJ, 932, 84
Michaely, E., & Perets, H. B. 2020, MNRAS, 498, 4924
Moe, M., & Di Stefano, R. 2017, ApJS, 230, 15
Müller, B., Viallet, M., Heger, A., & Janka, H.-T. 2016, ApJ, 833, 124
Mushkin, J., & Katz, B. 2020, MNRAS, 498, 665
Nagarajan, P., El-Badry, K., Chawla, C., et al. 2025, PASP, 137, 044202
Naoz, S., & Fabrycky, D. C. 2014, ApJ, 793, 137
Naoz, S., Farr, W. M., Lithwick, Y., Rasio, F. A., & Teyssandier, J. 2013a,
   MNRAS, 431, 2155
Naoz, S., Fragos, T., Geller, A., Stephan, A. P., & Rasio, F. A. 2016, ApJL,
  822. L24
Naoz, S., Kocsis, B., Loeb, A., & Yunes, N. 2013b, ApJ, 773, 187
Naoz, S., Li, G., Zanardi, M., de Elía, G. C., & Di Sisto, R. P. 2017, AJ,
   154, 18
Naoz, S., Will, C. M., Ramirez-Ruiz, E., et al. 2020, ApJL, 888, L8
Nutzman, P., Kalogera, V., Finn, L. S., Hendrickson, C., & Belczynski, K.
   2004, ApJ, 612, 364
Offner, S. S. R., Moe, M., Kratter, K. M., et al. 2023, in ASP Conf. Ser. 534,
   Protostars and Planets VII, ed. S. Inutsuka, Y. Aikawa, T. Muto,
   K. Tomida, & M. Tamura (San Francisco, CA: ASP), 275
O'Leary, R. M., Kocsis, B., & Loeb, A. 2009, MNRAS, 395, 2127
Payne, A. V., Shappee, B. J., Hinkle, J. T., et al. 2021, ApJ, 910, 125
Perets, H. B., Li, Z., Lombardi, J. C., Jr., & Milcarek, S. R., Jr. 2016, ApJ,
   823, 113
Perley, D. A., Mazzali, P. A., Yan, L., et al. 2019, MNRAS, 484, 1031
Peters, P. C. 1964, PhRv, 136, 1224
Peters, P. C., & Mathews, J. 1963, PhRv, 131, 435
Petrovich, C., & Antonini, F. 2017, ApJ, 846, 146
Press, W. H., & Teukolsky, S. A. 1977, ApJ, 213, 183
```

Remillard, R. A., & McClintock, J. E. 2006, AAS Meeting, 209, 07.05

```
Repetto, S., Davies, M. B., & Sigurdsson, S. 2012, MNRAS, 425, 2799
Rodriguez, C. L., Amaro-Seoane, P., Chatterjee, S., et al. 2018, PhRvD, 98,
  123005
Rodriguez, C. L., Chatterjee, S., & Rasio, F. A. 2016, PhRvD, 93, 084029
Rodriguez, C. L., Morscher, M., Pattabiraman, B., et al. 2015, PhRvL, 115,
Rose, S. C., Naoz, S., Sari, R., & Linial, I. 2022, ApJL, 929, L22
Ryu, T., de Mink, S. E., Farmer, R., et al. 2024, MNRAS, 527, 2734
Ryu, T., Perna, R., Pakmor, R., et al. 2023, MNRAS, 519, 5787
Ryu, T., Perna, R., & Wang, Y.-H. 2022, MNRAS, 516, 2204
Sahu, K. C., Anderson, J., Casertano, S., et al. 2022, ApJ, 933, 83
Samsing, J. 2018, PhRvD, 97, 103014
Samsing, J., Bartos, I., D'Orazio, D. J., et al. 2022, Natur, 603, 237
Shariat, C., El-Badry, K., & Naoz, S. 2025a, PASP, 137, 094201
Shariat, C., Naoz, S., El-Badry, K., et al. 2025b, ApJ, 983, 115
Shenar, T., Sana, H., Mahy, L., et al. 2022, NatAs, 6, 1085
Silsbee, K., & Tremaine, S. 2017, ApJ, 836, 39
Soderhjelm, S. 1975, A&A, 42, 229
Stephan, A. P., Naoz, S., Ghez, A. M., et al. 2019, ApJ, 878, 58
Stevenson, S., Berry, C. P. L., & Mandel, I. 2017, MNRAS, 471, 2801
Tagawa, H., Haiman, Z., & Kocsis, B. 2020, ApJ, 898, 25
Tagawa, H., Kimura, S. S., Haiman, Z., Perna, R., & Bartos, I. 2024, ApJ,
  966, 21
The LIGO Scientific Collaboration, the Virgo Collaboration & the KAGRA
  Collaboration 2025, arXiv:2508 18083
Thompson, T. A., Kochanek, C. S., Stanek, K. Z., et al. 2019, Sci, 366, 637
Tory, M., Grishin, E., & Mandel, I. 2022, PASA, 39, e062
Tremaine, S. 2023, MNRAS, 522, 937
Tsuna, D., & Lu, W. 2025, ApJ, 986, 84
van Son, L. A. C., Roy, S. K., Mandel, I., et al. 2025, ApJ, 979, 209
Veronesi, N., van Velzen, S., & Rossi, E. M. 2025, MNRAS, 536, 3112
Vigna-Gómez, A. 2025, A&A, 701, L3
Vigna-Gómez, A., Toonen, S., Ramirez-Ruiz, E., et al. 2021, ApJL,
Vigna-Gómez, A., Willcox, R., Tamborra, I., et al. 2024, PhRvL, 132, 191403
Vinson, B. R., & Chiang, E. 2018, MNRAS, 474, 4855
Vynatheya, P., Hamers, A. S., Mardling, R. A., & Bellinger, E. P. 2022,
          S, 516, 4146
Weldon, G. C., Naoz, S., & Hansen, B. M. S. 2024, ApJ, 974, 302
Wiktorowicz, G., Wyrzykowski, Ł., Chruslinska, M., et al. 2019, ApJ, 885, 1
Will, C. M. 2017, PhRvD, 96, 023017
Will, C. M. 2021, PhRvD, 103, 063003
Willcox, R., Marchant, P., Vigna-Gómez, A., et al. 2025, A&A, 700, A59
Wu, Y. 2018, AJ, 155, 118
Xin, C., Haiman, Z., Perna, R., Wang, Y., & Ryu, T. 2024, ApJ, 961, 149
Yang, Y., Bartos, I., Fragione, G., et al. 2022, ApJL, 933, L28
Zanardi, M., de Elía, G. C., Di Sisto, R. P., et al. 2017, A&A, 605, A64
Zevin, M., Bavera, S. S., Berry, C. P. L., et al. 2021, ApJ, 910, 152
Zhang, E., Naoz, S., & Will, C. M. 2023, ApJ, 952, 103
```